Measuring Spin of the Remnant Black Hole from Maximum Amplitude

Deborah Ferguson¹, Sudarshan Ghonge¹, James A. Clark¹, Juan Calderon Bustillo^{2,3}, Pablo Laguna¹, and Deirdre Shoemaker ¹

¹Center for Relativistic Astrophysics and School of Physics, Georgia Institute of Technology, Atlanta, GA 30332

²Monash Centre for Astrophysics, School of Physics and Astronomy, Monash University, VIC 3800, Australia ³OzGrav: The ARC Centre of Excellence for Gravitational-Wave Discovery, Clayton, VIC 3800, Australia

Gravitational waves emitted during the merger of two black holes carry information about the remnant black hole, namely its mass and spin. This information is typically found from the ringdown radiation as the black hole settles to a final state. We find that the remnant black hole spin is already known at the peak amplitude of the gravitational wave strain. Using this knowledge, we present a new method for measuring the final spin that is template independent, using only the chirp mass, the instantaneous frequency of the strain and its derivative at maximum amplitude, all template independent.

PACS numbers: 04.80.Nn, 04.25.dg, 04.25.D-, 04.30.-w

INTRODUCTION

The advent of gravitational wave (GW) astronomy has granted us the opportunity to observationally study compact binary coalescences. During the course of the first two observing runs, LIGO [1] and Virgo [2] detected GWs from a total of ten coalescing binary black holes (BBHs) and one binary neutron star [3, 4]. These systems have hinted at the population properties of BBHs such as the distributions of mass, spin and redshifts [5], and have placed GW observations into the new era of multi-messenger astronomy [4, 6].

In the few years since the first detection of GWs [7], we have learned a tremendous amount about the parameter space of stellar-mass black holes (BHs) [5]. Each stage of the coalescence provides information about the BBH system; this study focuses on the parameters describing the remnant BH. The product of a BBH merger is a perturbed BH that emits ringdown radiation as it settles to a Kerr BH. This process provides fundamental information to understand gravity in its most extreme regime. Perturbation theory tells a compelling story about how perturbed BHs, like the remnant of a BBH merger, lose the information about the disturbance, often called hair. in the form of GWs [8]. Perturbed BHs ring down or emit GWs with a frequency (ω_{qnm}) and decay time (τ_{qnm}) characterized by the BH mass and spin [9], providing the means to determine the remnant BH parameters upon the detection of GWs.

The GW during this ringdown phase is generally represented as the sum of quasi-normal modes (QNMs), each expressible as a damped sinusoid with its own ω_{qnm} and τ_{qnm} , fixed by the mass and spin of the final BH [10–12]. The Echeverria formulas [13] provide relationships to determine the BH mass and spin from ω_{qnm} and τ_{qnm} using spheroidal harmonics.

There have been attempts to measure ω_{qnm} and τ_{qnm} of the ringdown [14–20] and as the detectors improve in

sensitivity, this will become more viable. One commonly considered method is to estimate the ringdown parameters by matching directly to the exponentially decaying ringdown, where Ref.[17] finds consistent results for GW150914 searching for damped sinusoids. The possibility of using GWs to detect this spectrum of radiation is often referred to as BH spectroscopy [21–23]. The short duration and low-amplitude of the signal expected from stellar-mass mergers, however, makes this post-merger phase challenging to detect, which is further compounded by the reliance upon knowing when ringdown begins [24, 25].

Due to these challenges, current approaches [26–28] to estimate the spin of the final BH match the data to theoretical models of the inspiral. Fortunately, numerical relativity (NR) provides the map from initial to final parameters [29–31] that are used to estimate the final spin. For systems with many cycles of inspiral, this method can predict the remnant spin with precision, assuming general relativity (GR). It is desirable to obtain the remnant spin independently of matched filtering of either the inspiral or ringdown in order to perform tests of GR [26, 32–34]. One can also perform tests of GR directly from the peak frequency [35].

With the goal of avoiding the use of the exponentially decaying ringdown, we propose a method of determining the final spin that takes advantage of the higher amplitude at the merger of two BHs. The method proposed here builds on earlier work by Healy et~al~[36] which connected the instantaneous frequency of the GW at peak amplitude to ω_{qnm} and τ_{qnm} of the ringdown. While it is not obvious that such a relationship should exist, there have been hints of the merged black hole entering a perturbative regime as early as the peak amplitude [36–39] with the radiation near the peak amplitude of the strain being described by QNMs that include the overtones. In this paper, we find that the spin of the remnant black hole is already known at the peak amplitude.

Inspired by the results of Healy et~al, we create a map linking the instantaneous frequency at maximum amplitude (ω_{peak}) , the derivative of the instantaneous frequency at maximum amplitude $(\dot{\omega}_{peak})$, and the chirp mass (\mathcal{M}) to the dimensionless remnant spin (a_f) . One advantage of this method is that all measurements involved, ω_{peak} , $\dot{\omega}_{peak}$, and \mathcal{M} , are independent of fitting the data to a model waveform. Furthermore, \mathcal{M} has the advantage of needing only a few pre-peak cycles to obtain a good measurement using a well known gravitational-wave algorithm, Coherent WaveBurst (cWB) [40]. In the following we: a) demonstrate a tight relation between the frequency properties measured at peak and the spin of the final BH and b) develop an algorithm to exploit this relationship on GW observations.

In the Methodology section, we describe the NR data used to derive a connection from ω_{peak} , $\dot{\omega}_{peak}$, \mathcal{M} to a_f and discuss the associated errors. In the Final Spin section, we examine the viability of the relationship as a form of parameter estimation with noisy data. Finally, we summarize our findings in the Conclusions section.

METHODOLOGY

NR Catalog and Errors

The relationships found in this paper are based upon the use of 112 NR simulations provided by the Georgia Tech waveform catalog, 47 of which are nonspinning and 65 of which are aligned spin, with mass ratios 1 < q < 10 [41]. The Georgia Tech waveforms are produced using the MAYA code [42–45], a branch of the Einstein Toolkit [46], a NR code built upon Cactus with mesh refinement from Carpet [47] with the addition of thorns to calculate various quantities during the simulation including an apparent horizon solver [48].

We create a map from ω_{peak} , $\dot{\omega}_{peak}$, \mathcal{M} to a_f . As will be described in subsection "Fitting to final spin," this equates to a mapping from the dimensionless instantaneous frequency at maximum amplitude $(\hat{\omega}_{peak})$, the derivative of the dimensionless instantaneous frequency at maximum amplitude $(\hat{\omega}_{peak})$, and the symmetric mass ratio (η) to a_f .

In order to create this mapping, $\hat{\omega}_{peak}$, $\hat{\omega}_{peak}$, and a_f are obtained from the NR simulation data. In this paper we use the strain, h(t), for ease of working with the GW detectors, given

$$h(t) = h_{+}(t) - ih_{\times}(t) = \int_{-\infty}^{t} dt' \int_{-\infty}^{t'} dt'' \psi_{4}(t''),$$

and computed according to [49]. Strain is represented as a sum of spin-weighted spherical harmonics $_{-2}Y_{\ell,m}$ given

by

$$h(t, \theta, \phi) = \sum_{\ell, m} {}_{-2}Y_{\ell, m}(\theta, \phi)h_{\ell, m}(t),$$

where $h_{\ell,m}$ are excited depending on the inspiral parameters and the binary's orientation with respect to the observer. In aligned spin scenarios and face on orientations, the $\ell = 2$, m=2 mode dominates the signal; and, therefore, this study uses only the $\ell = 2$, m = 2 mode [50–53].

The GW amplitude is thus $|h_{22}(t)|$, and the instantaneous frequency is found as the derivative of the phase, i.e. $\dot{\phi}(t)$ where $\phi(t) = arg(h_{22}(t))$. $\hat{\omega}_{peak}$ and $\hat{\omega}_{peak}$ are obtained simply by identifying the time at which the amplitude reaches a maximum and grabbing the instantaneous frequency and its time derivative at that time. This is shown visually in Fig. 1. Note a_f is determined

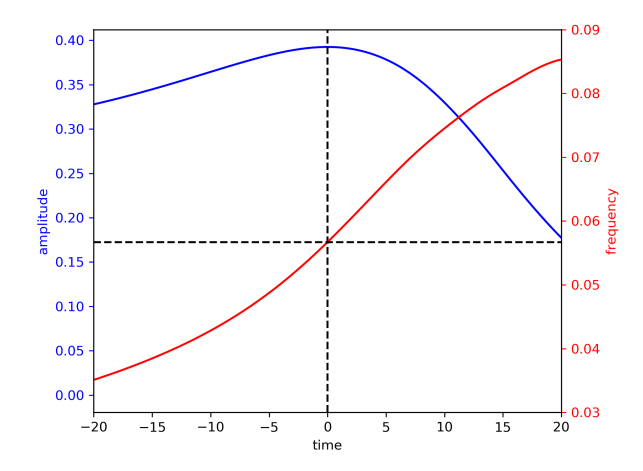


FIG. 1: The figure depicts the amplitude and the frequency during merger. The vertical dotted line denotes the time of maximum amplitude and the horizontal dotted line shows the corresponding instantaneous frequency.

from the apparent horizon of the remnant BH.

The finite spatial and temporal resolutions of NR simulations introduce systematic uncertainty into the estimates of frequency and spin. By repeating each simulation at multiple resolutions, the error is found to be of order 0.01% for a_f , 1% for $\hat{\omega}_{peak}$, and 1.4% for $\hat{\omega}_{peak}$. These uncertainties account for the spread in the fit shown in Fig. 2.

Fitting to final spin

With the data selected and the NR errors understood, we can create a fit that connects the peak amplitude of GW strain to the final BH spin. In order to create this fitting from ω_{peak} , $\dot{\omega}_{peak}$, and \mathcal{M} to a_f using NR simulations, we utilize the following relationships

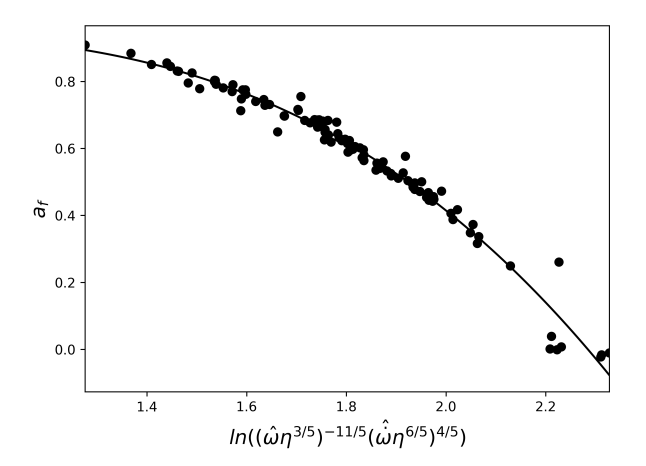


FIG. 2: We plot the dimensionless spin of the remnant black hole versus a function of symmetric mass ratio, instantaneous dimensionless frequency, and its time derivative at maximum strain for aligned spin numerical relativity waveforms. The solid line shows the fitting relation described in the "Fitting to final spin" subsection.

$$\hat{\omega}\eta^{\frac{3}{5}} = \omega \mathcal{M} \tag{1}$$

$$\hat{\omega}\eta^{\frac{6}{5}} = \dot{\omega}\mathcal{M}^2 \tag{2}$$

where η is the symmetric mass ratio defined as a function of the initial masses, m_1 and m_2 :

$$\eta = \frac{m_1 m_2}{(m_1 + m_2)^2} \,, \tag{3}$$

and \mathcal{M} is the chirp mass expressible as:

$$\mathcal{M} = \eta^{\frac{3}{5}} M = \frac{c^3}{G} \left(\frac{5}{96} \pi^{-\frac{8}{3}} f^{-\frac{11}{3}} \dot{f} \right)^{\frac{3}{5}} . \tag{4}$$

These lead us to plot the spin of the remnant BH against a function of $\hat{\omega}_{peak}\eta^{\frac{3}{5}}$ and $\hat{\omega}_{peak}\eta^{\frac{6}{5}}$ which will take the form

$$x = \ln\left(\left(\hat{\omega}_{\text{peak}}\eta^{\frac{3}{5}}\right)^{-\frac{11}{5}}\left(\hat{\omega}_{\text{peak}}\eta^{\frac{6}{5}}\right)^{\frac{4}{5}}\right). \tag{5}$$

The resulting fit is shown in Fig 2. Adopting the same functional form as Healy et.al~[36], we obtain the following best fit relationship

$$a_f = -0.216x^3 + 0.415x^2 - 0.252x + 0.989$$
 (6)

with an average spread of $\Delta a_f = 0.032$.

FINAL SPIN

Having found an NR derived relationship relating ω_{peak} , $\dot{\omega}_{peak}$, and \mathcal{M} to a_f , it's important to study how these values are obtained from real data and how precise this method will be when faced with a detection. \mathcal{M} is measured by burst searches that fit the frequency evolution of the signal [40]. By analyzing the recovered \mathcal{M} of existing cWB runs, and using the knowledge that the uncertainty scales as 1/signal-to-noise ratio (SNR) [54], we estimate that the uncertainty in \mathcal{M} as recovered by cWB is $\sim 1.5/\text{SNR}$. This contributes an additional uncertainty of (126/SNR) % to a_f . For the SNR=100 runs we analyze in this paper, this adds an uncertainty of 1.26% to a_f .

Since GW detector data is noisy, we can't reliably obtain ω_{peak} and $\dot{\omega}_{peak}$ directly without first de-noising it. In order to reconstruct a signal out of the noise, we use BayesWave, a search pipeline that relies on modeling the GW as a number of sine Gaussians whose sum results in a coherent GW signal in a detector network [55]. By using this morphology-agnostic approach, the reconstructed waveform is robust against uncertainties which may be present in templated analyses. The latter model the waveform based on the time orbital evolution of Compact Binary Coalescences and are hence often referred to as CBC analyses [56]. BayesWave provides an independent, complementary estimate of the waveform morphology, and consequently avoids systematic uncertainty in the frequency evolution which might be present in the best fit CBC waveform [57, 58]. In this study we analyze the waveform as reconstructed by BayesWave for the Livingston detector only.

To quantify the expected uncertainty in the remnant spin, we performed a systematic Monte-Carlo study whereby sets of BBH signals with increasing SNR [59] were added to stationary Gaussian noise colored with the power spectral density of O1 era LIGO detectors. The underlying waveforms for these "injections" were then recovered using BayesWave. For a SNR of 100, we injected a h_{22} signal consistent with that of GW150914 in 2000 realizations of Gaussian noise and recovered ω_{peak} and $\dot{\omega}_{peak}$ for the median waveform of each. The value of ω_{peak} was obtained by first calculating the amplitude envelope of the median whitened waveform (using a python implementation of the Hilbert-Huang transform [60]) and then locating the time at which the amplitude is maximum. Then the median time frequency track, outputted by BayesWave, is used to identify the frequency and the time derivative of the frequency at the given time.

Fig 3 shows the cumulative probability distribution of the estimated a_f for our 2000 injections. The solid black line denotes the median, the solid red line denotes the true final spin, and the dotted lines show the 90% confidence interval, which is $a_f = (0.51, 0.77)$ for SNR of 100.

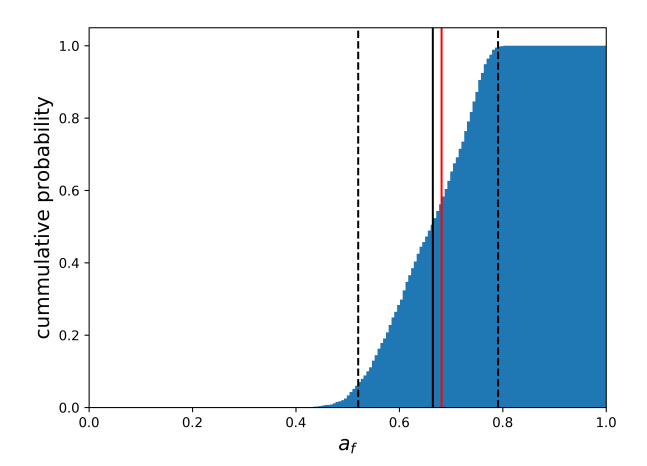


FIG. 3: We plot the cumulative probability distribution of the final dimensionless spin obtained for a GW150914-like signal injected into noise and recovered using BayesWave with SNR 100. The solid black line shows the median recovered spin and the dotted black lines show the 90% confidence interval. The solid red line shows the true spin.

To better understand how this error scales with SNR, we used the same technique just described with 250 injections each for SNRs 40, 60, 80, and 100. The resulting medians and 90% confidence intervals are shown in Table I.

SNR	median	lower 90% confidence	upper 90% confidence
40	0.671	0.437	0.802
60	0.677	0.484	0.785
80	0.654	0.497	0.782
100	0.667	0.510	0.772

TABLE I: Median and 90% confidence values of a_f for various SNRs

CONCLUSIONS

This study finds that the remnant spin is known at the peak amplitude and presents a method of estimating it from the chirp mass, the frequency at maximum amplitude of the strain, and its derivative in an analytic relationship. This allows us to make use of the high SNR at the peak to estimate the final spin before entering the perturbative ringdown regime.

In order to understand the viability of this study as a parameter estimation method, we analyzed the distribution of the remnant spin obtained via recovering the waveform of a GW150914-like signal with increasing SNRs from 40 to 100. We demonstrate that we can reliably place bounds on the spin of the remnant BH using information found near the peak amplitude when the

signal is dominated by the $\ell = 2$, m = 2 mode.

Our method avoids the usage of BBH templates, instead obtaining ω_{peak} and $\dot{\omega}_{peak}$ from a BayesWave reconstruction and \mathcal{M} from cWB. While matched filtering methods likely place a tighter bound on the remnant spin, our alternate approach is not subject to the same systematic biases due to waveform modeling present in the matched filter search. There remain systematic errors due to the fit we are using to determine the final spin from the peak amplitude. In addition, the fitting formula is an interpolation over a discrete set of NR templates and might change if more NR simulations are added to the fit.

Next steps in this study will see the method applied to all the LIGO/VIRGO BBH detections with reasonable BayesWave reconstructions from O1, O2 and, soon, O3. It will also be interesting to see the effect of adding precessing runs to the fit and whether this analysis can be expanded to include higher modes.

Acknowledgements PL and DS gratefully acknowledge support from the NSF grants PHY-1806580, PHY-1809572, PHY-1550461 and 1333360, XSEDE TG-PHY120016. JCB also acknowledges support from Australian Research Council Discovery Project DP180103155. This research was also supported in part through research cyberinfrastructure resources and services provided by the Partnership for an Advanced Computing Environment (PACE) at the Georgia Institute of Technology. The authors are grateful for computational resources provided by the LIGO Laboratory and supported by National Science Foundation Grants PHY-0757058 and PHY-0823459. We also thank Karan Jani for useful discussions.

- J. Aasi et al. (LIGO Scientific), Class. Quant. Grav. 32, 074001 (2015), arXiv:1411.4547 [gr-qc].
- [2] F. Acernese et al. (VIRGO), Class. Quant. Grav. 32, 024001 (2015), arXiv:1408.3978 [gr-qc].
- [3] The LIGO Scientific Collaboration and the Virgo Collaboration, arXiv e-prints, arXiv:1811.12907 (2018), 1811.12907 [astro-ph.HE].
- [4] L. S. Collaboration and V. Collaboration, Phys. Rev. Lett. 119, 161101 (2017).
- [5] The LIGO Scientific Collaboration and The Virgo Collaboration, arXiv e-prints, arXiv:1811.12940 (2018), 1811.12940 [astro-ph.HE].
- [6] P. Maészàros, D. B. Fox, C. Hanna, and K. Murase, (2019), arXiv:1906.10212 [astro-ph.HE].
- [7] L. S. Collaboration and V. Collaboration, Phys. Rev. Lett. 116, 061102 (2016).
- [8] C. V. Vishveshwara, Phys. Rev. D 1, 2870 (1970).
- [9] W. H. Press, ApJ Letters **170**, L105 (1971).
- [10] H.-P. Nollert and R. H. Price, Journal of Mathematical Physics 40, 980 (1999), arXiv:gr-qc/9810074 [gr-qc].
- [11] K. D. Kokkotas and B. G. Schmidt, Living Reviews in Relativity 2, 2 (1999), arXiv:gr-qc/9909058 [gr-qc].

- [12] E. Berti, V. Cardoso, and A. O. Starinets, Classical and Quantum Gravity 26, 163001 (2009), arXiv:0905.2975 [gr-qc].
- [13] F. Echeverria, Phys. Rev. D 40, 3194 (1989).
- [14] B. P. Abbott et al. (LIGO Scientific), Phys. Rev. D80, 062001 (2009), arXiv:0905.1654 [gr-qc].
- [15] L. M. Goggin and the LIGO Scientific Collaboration, Classical and Quantum Gravity 23, S709 (2006).
- [16] E. Berti, J. Cardoso, V. Cardoso, and M. Cavaglia, Phys. Rev. D76, 104044 (2007), arXiv:0707.1202 [gr-qc].
- [17] G. Carullo, W. Del Pozzo, and J. Veitch, arXiv:1902.07527 (2019).
- [18] H. Yang, K. Yagi, J. Blackman, L. Lehner, V. Paschalidis, F. Pretorius, and N. Yunes, Phys. Rev. Lett. 118, 161101 (2017).
- [19] H. Nakano, T. Narikawa, K.-i. Oohara, K. Sakai, H.-a. Shinkai, H. Takahashi, T. Tanaka, N. Uchikata, S. Yamamoto, and T. S. Yamamoto, (2018), arXiv:1811.06443 [gr-qc].
- [20] M. Cabero, C. D. Capano, O. Fischer-Birnholtz, B. Krishnan, A. B. Nielsen, A. H. Nitz, and C. M. Biwer, Phys. Rev. D 97, 124069 (2018).
- [21] O. Dreyer, B. J. Kelly, B. Krishnan, L. S. Finn, D. Garrison, and R. Lopez-Aleman, Class. Quant. Grav. 21, 787 (2004), arXiv:gr-qc/0309007 [gr-qc].
- [22] E. Berti, V. Cardoso, and C. M. Will, Phys. Rev. D73, 064030 (2006), arXiv:gr-qc/0512160 [gr-qc].
- [23] R. Brito, A. Buonanno, and V. Raymond, Phys. Rev. D 98, 084038 (2018).
- [24] S. Bhagwat, M. Okounkova, S. W. Ballmer, D. A. Brown, M. Giesler, M. A. Scheel, and S. A. Teukolsky, Phys. Rev. **D97**, 104065 (2018), arXiv:1711.00926 [gr-qc].
- [25] G. Carullo, L. van der Schaaf, L. London, P. T. H. Pang, K. W. Tsang, O. A. Hannuksela, J. Meidam, M. Agathos, A. Samajdar, A. Ghosh, T. G. F. Li, W. Del Pozzo, and C. Van Den Broeck, Phys. Rev. D 98, 104020 (2018).
- [26] B. P. Abbott et al. (Virgo, LIGO Scientific), Phys. Rev. Lett. 116, 221101 (2016), [Erratum: Phys. Rev. Lett.121,no.12,129902(2018)], arXiv:1602.03841 [gr-qc].
- [27] J. Healy, C. O. Lousto, and Y. Zlochower, Phys. Rev. D90, 104004 (2014), arXiv:1406.7295 [gr-qc].
- [28] L. Rezzolla, P. Diener, E. N. Dorband, D. Pollney, C. Reisswig, E. Schnetter, and J. Seiler, Astrophys. J. 674, L29 (2008), arXiv:0710.3345 [gr-qc].
- [29] J. Healy and C. O. Lousto, PRD 95, 024037 (2017), arXiv:1610.09713 [gr-qc].
- [30] X. Jiménez-Forteza, D. Keitel, S. Husa, M. Hannam, S. Khan, and M. Pürrer, PRD 95, 064024 (2017), arXiv:1611.00332 [gr-qc].
- [31] F. Hofmann, E. Barausse, and L. Rezzolla, ApJL 825, L19 (2016), arXiv:1605.01938 [gr-qc].
- [32] B. P. Abbott et al. (LIGO Scientific, Virgo), (2019), arXiv:1903.04467 [gr-qc].
- [33] A. Ghosh, N. K. Johnson-Mcdaniel, A. Ghosh, C. K. Mishra, P. Ajith, W. Del Pozzo, C. P. L. Berry, A. B. Nielsen, and L. London, Class. Quant. Grav. 35, 014002 (2018), arXiv:1704.06784 [gr-qc].
- [34] A. Ghosh et al., Phys. Rev. **D94**, 021101 (2016), arXiv:1602.02453 [gr-qc].
- [35] G. Carullo, G. Riemenschneider, K. W. Tsang, A. Nagar, and W. Del Pozzo, Class. Quant. Grav. 36, 105009 (2019), arXiv:1811.08744 [gr-qc].
- [36] J. Healy, P. Laguna, and D. Shoemaker, Classical and Quantum Gravity 31, 212001 (2014), arXiv:1407.5989

- [gr-qc].
- [37] A. Buonanno, G. B. Cook, and F. Pretorius, Phys. Rev. D75, 124018 (2007), arXiv:gr-qc/0610122 [gr-qc].
- [38] I. Kamaretsos, M. Hannam, and B. S. Sathyaprakash, Phys. Rev. Lett. 109, 141102 (2012).
- [39] M. Giesler, M. Isi, M. Scheel, and S. Teukolsky, (2019), arXiv:1903.08284 [gr-qc].
- [40] V. Tiwari, S. Klimenko, V. Necula, and G. Mitselmakher, Class. Quant. Grav. 33, 01LT01 (2016), arXiv:1510.02426 [astro-ph.IM].
- [41] K. Jani, J. Healy, J. A. Clark, L. London, P. Laguna, and D. Shoemaker, Classical and Quantum Gravity 33, 204001 (2016), arXiv:1605.03204 [gr-qc].
- [42] F. Herrmann, I. Hinder, D. Shoemaker, and P. Laguna, Classical and Quantum Gravity 24, S33 (2007), arXiv:gr-qc/0601026 [gr-qc].
- [43] B. Vaishnav, I. Hinder, F. Herrmann, and D. Shoemaker, Phys. Rev. D 76, 084020 (2007), arXiv:0705.3829 [gr-qc].
- [44] J. Healy, J. Levin, and D. Shoemaker, Phys. Rev. Lett. 103, 131101 (2009).
- [45] L. Pekowsky, R. O'Shaughnessy, J. Healy, and D. Shoemaker, Phys. Rev. D 88, 024040 (2013).
- [46] F. Loffler et al., Class. Quant. Grav. 29, 115001 (2012), arXiv:1111.3344 [gr-qc].
- [47] E. Schnetter, S. H. Hawley, and I. Hawke, Class. Quant. Grav. 21, 1465 (2004), arXiv:gr-qc/0310042 [gr-qc].
- [48] J. Thornburg, Class. Quant. Grav. 21, 743 (2004), arXiv:gr-qc/0306056 [gr-qc].
- [49] C. Reisswig and D. Pollney, Class. Quant. Grav. 28, 195015 (2011), arXiv:1006.1632 [gr-qc].
- [50] J. Caldern Bustillo, P. Laguna, and D. Shoemaker, Phys. Rev. **D95**, 104038 (2017), arXiv:1612.02340 [gr-qc].
- [51] J. Caldern Bustillo, S. Husa, A. M. Sintes, and M. Prrer, Phys. Rev. **D93**, 084019 (2016), arXiv:1511.02060 [gr-qc].
- [52] L. Pekowsky, J. Healy, D. Shoemaker, and P. Laguna, Phys. Rev. D87, 084008 (2013), arXiv:1210.1891 [gr-qc].
- [53] V. Varma and P. Ajith, Phys. Rev. D96, 124024 (2017), arXiv:1612.05608 [gr-qc].
- [54] M. Vallisneri, Phys. Rev. D77, 042001 (2008), arXiv:gr-qc/0703086 [GR-QC].
- [55] N. J. Cornish and T. B. Littenberg, Class. Quant. Grav. 32, 135012 (2015), arXiv:1410.3835 [gr-qc].
- [56] S. Fairhurst and P. Brady, Class. Quant. Grav. 25, 105002 (2008).
- [57] J. Veitch, V. Raymond, B. Farr, W. Farr, P. Graff, S. Vitale, B. Aylott, K. Blackburn, N. Christensen, M. Coughlin, et al., Physical Review D 91, 042003 (2015).
- [58] C. Messick, K. Blackburn, P. Brady, P. Brockill, K. Cannon, R. Cariou, S. Caudill, S. J. Chamberlin, J. D. E. Creighton, R. Everett, C. Hanna, D. Keppel, R. N. Lang, T. G. F. Li, D. Meacher, A. Nielsen, C. Pankow, S. Privitera, H. Qi, S. Sachdev, L. Sadeghian, L. Singer, E. G. Thomas, L. Wade, M. Wade, A. Weinstein, and K. Wiesner, Phys. Rev. D 95, 042001 (2017), arXiv:1604.04324 [astro-ph.IM].
- [59] E. Parzen, IEEE Trans. Inf. Theor. 9, 127 (2006).
- [60] N. E. Huang, Z. Shen, S. R. Long, M. C. Wu, H. H. Shih, Q. Zheng, N.-C. Yen, C. C. Tung, and H. H. Liu, Proceedings of the Royal Society of London. Series A: Mathematical, Physical and Engineering Sciences 454, 903 (1998), https://royalsocietypublishing.org/doi/pdf/10.1098/rspa.1998.0193.